Spin density wave order in interacting type-I and type-II Weyl semimetals

Sarbajaya Kundu* and David Sénéchal
Département de Physique and Institut Quantique, Université de Sherbrooke, Sherbrooke, Québec, Canada J1K 2R1

(Received 13 October 2020; accepted 10 February 2021; published 23 February 2021)

Weyl semimetals, featuring massless linearly dispersing chiral fermions in three dimensions, provide an excellent platform for studying the interplay of electronic interactions and topology, and exploring new correlated states of matter. Here, we examine the effect of a local repulsive interaction on an inversion-symmetry breaking Weyl semimetal model, using cluster dynamical mean-field theory and variational cluster approximation methods. Our analysis reveals a continuous transition from the gapless Weyl semimetal phase to a gapped spin density wave ordered phase at a critical value of the interaction, which is determined by the band structure parameters. Further, we introduce a finite tilt in the linear dispersion and examine the corresponding behavior for a type-II Weyl semimetal model, where the critical interaction strength is found to be significantly diminished, indicating a greater susceptibility towards interactions. The behavior of different physical quantities, such as the double occupancy, the spectral function, and the Berry curvature, associated with the Weyl nodes, is obtained in both the semimetallic and the magnetically ordered states. Finally, we provide an interaction-induced phase diagram for the Weyl semimetal model, as a function of the tilt parameter.

DOI: 10.1103/PhysRevB.103.085136

I. INTRODUCTION

The interplay of electronic correlations and band topology in strongly spin-orbit coupled systems [1–3] has generated considerable interest in contemporary condensed-matter physics, with the potential to uncover new and exotic phases of matter. In this context, topological insulators [4–10] and Weyl semimetals [11–14] are examples of strongly spin-orbit coupled systems with low-energy degrees of freedom that are described by massless linearly dispersing electrons, and are suitable for studying the combination of many-body and band structure effects in topological materials. In particular, Weyl semimetals (WSMs) feature pairs of nondegenerate bands touching each other at isolated points in the band structure, with Weyl fermions as low-energy quasiparticles. Theoretically, this can be realized by breaking either inversion or time-reversal symmetry (TRS), or both. WSMs are characterized by open Fermi arcs [13,15–20] on their surfaces and a novel response to applied electric and magnetic fields [13,21–26]. A conventional or type-I Weyl semimetal has a conical spectrum and a pointlike Fermi surface, but the energy dispersion at the node could also be tilted along a given direction. When the tilt exceeds a certain critical value, the Weyl node appears at the intersection of an electron and a hole pocket, giving rise to a type-II WSM [15,27–29]. The latter class of models is known to have properties qualitatively different from those of the former, some of which include a field-selective anomaly in magnetotransport [30] and an intrinsic anomalous Hall effect [31]. On the experimental side, a number of material candidates for both type-I and type-II Weyl semimetals have been proposed, and confirmed in recent times [15,20,28,32–37].

Correlation effects are expected to be important for Weyl semimetal candidates, which often involve heavier elements with a strong spin-orbit interaction. Moreover, there have been experimental reports of collective many-body effects, such as superconductivity [33,38] or magnetism [39,40], in Weyl semimetals, necessitating the theoretical treatment of electronic instabilities. Other important questions include the robustness of the topological properties of a Weyl semimetal in the presence of interactions [41–46], and the possibility of realizing interaction-induced topologically nontrivial phases [42,43]. The effects of electronic interactions in WSMs have been explored using various approaches [41–60] such as perturbative renormalization group (RG) [50–52,56,57,61], mean-field analyses [29,44,48,49,53,54,62], strong-coupling expansion methods [42], and, occasionally, numerical techniques [43,45,46,55]. Specific examples of possible broken-symmetry states have been considered, such as excitonic and charge density wave (CDW) instabilities [42–44,49,50,54,56], as well as superconducting ground states [29,48,63,64]. There have been comparatively fewer studies of interaction effects in type-II WSMs, generally using similar approaches [53,56,65]. In order to complement the existing results, it is useful to employ a nonperturbative approach, which can describe the physical properties of the model by continuously varying the interaction strength, producing results that are highly illustrative and comprehensive in nature. Besides, having a common framework to detect possible broken-symmetry phases and examine the changes in the topological properties of the system makes it easier to characterize new and exotic types of order. Finally, one needs a simple way of introducing a linear tilt in the dispersion and examining its effect on the properties of the interacting WSM model.

In this paper, we attempt to address these concerns by studying the effect of a local, repulsive interaction on a simple inversion-symmetry breaking Weyl semimetal model, using

*Corresponding author: sarbajaya.kundu@usherbrooke.ca

two complementary methods: cluster dynamical mean-field theory (CDMFT) [66–69] and the variational cluster approximation (VCA) [43,70–73]. Both of these belong to a set of closely related approaches known as quantum cluster methods [74,75], which consider a finite cluster of sites embedded in an infinite lattice, and consider additional fields or "bath" degrees of freedom, so as to best represent the effect of the surrounding infinite lattice. The values of these additional parameters are decided using variational or self-consistency principles. In these approaches, broken-symmetry states can appear even for the smallest clusters used and, unlike ordinary mean-field theory, these are dynamical in nature and retain the full effect of strong correlations. These methods allow us to obtain the full interacting Green's function, spectral functions, and topological properties as a function of the interaction strength, and include additional tuning parameters, such as a finite tilt in the dispersion, with relative ease.

Our main findings are as follows. At a critical value of the interaction strength, $U = U_c$, the Weyl semimetal undergoes a continuous transition to a topologically trivial spin density wave (SDW) ordered state. We find an ordering wave vector $Q = (0, 0, \pi)$, which connects Weyl nodes of opposite chiralities, with the magnetization pointing in the z direction. In the rest of the paper, we denote this particular SDW order as $M_z^{(0,0,\pi)}$. For the untilted Weyl dispersion, it is equivalent to a state with an ordering wave vector $Q = (\pi, 0, 0)$ (see the Appendix), with the magnetization pointing in the x direction, which we henceforth denote as $M_x^{(\pi,0,0)}$. These particular orders are presumably favored by the presence of nesting in the band structure, between Weyl nodes of opposite chiralities. Since our analysis is limited to the effect of repulsive local interactions at half filling, we constrain our attention to various spin density wave instabilities. As expected, the magnetic order is accompanied by the gradual appearance of a spectral gap and the destruction of the Berry curvature associated with the Weyl nodes, which we compute for the folded band structure, in the ordered state. As the interaction amplitude increases, the SDW order is found to become more robust, as indicated by a gradual increase in the magnitude of the order parameter. The critical interaction U_c, at which it appears, also depends on the details of the band structure and the model parameters that are considered. We introduce a finite tilt parameter w_z (assumed to be along the k_z direction for simplicity) and find that in the overtilted type-II regime, the transition occurs at a significantly diminished value of the interaction, U_c. This is consistent with the expectation of an increased sensitivity towards interactions, when each Fermi point is replaced by an electron and a hole pocket [see Fig. 1(b)]. Once again, the SDW order $M_z^{(0,0,\pi)}$ (which is no longer equivalent to $M_x^{(\pi,0,0)}$ for $w_z \neq 0$) is found to be favored for the type-II WSM model. In general, the magnitude of the tilt parameter strongly affects the critical interaction amplitude for the transition, and its orientation may decide the specific nature of the SDW order. In particular, a different spin density wave order denoted as $M_z^{(\pi,\pi,\pi)}$, with an ordering wave vector $Q = (\pi, \pi, \pi)$, is also found to compete with $M_z^{(0,0,\pi)}$, for a more general direction of the tilt (see Figs. 9 and 10 for a pictorial depiction of the different types of magnetic order that can be realized in this system). We have independently verified our results for the order of the phase transition and the competing density wave instabilities, using both the CDMFT and the VCA approaches.

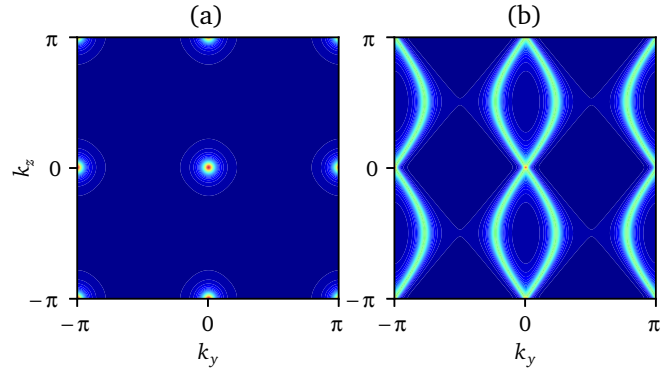

FIG. 1. Projection of the Fermi surface on the $k_x = 0$ plane, for the WSM model defined in Eq. (2), with band structure parameters $v_x = v_y = v_z = 1$, and (a) $w_z = 0$ (type-I) for $U = 1$, and (b) $w_z = 1.2$ (type-II) for $U = 0$. In the former case, we observe Fermi points at the positions of the Weyl nodes in the plane, i.e., (0,0,0), $(0, 0, \pm\pi)$, $(0, \pm\pi, 0)$, and $(0, \pm\pi, \pm\pi)$, whereas in the latter case, each Fermi point is replaced by an electron and a hole pocket, connected by the corresponding Weyl node, the boundaries of which can be clearly seen along the k_z direction. Note that we choose an interaction strength $U < U_c$ for the above illustration, where U_c is a critical value of the interaction amplitude, at which a gap opens in the spectrum and the system becomes magnetically ordered.

The paper is organized as follows. In Sec. II, we introduce the model Hamiltonian and provide a brief overview of the CDMFT and VCA methods that are used in our analysis. In Sec. III, we present the results of our CDMFT computations for the double occupancy and the dominant SDW order parameter, as a function of the interaction. We also pictorially illustrate the behavior of the spectral function and the Berry curvature associated with the Weyl nodes. We then present the results of our VCA calculations, which confirm the nature of the spin density wave instability occurring in this system, as well as the order of the transition. We also present the corresponding results as a function of the increasing tilt parameter w_z, which pushes the critical interaction strength U_c to smaller values. Based on these results, we present the interaction-induced phase diagram of the WSM model considered by us, as a function of w_z. Finally, in Sec. IV, we summarize our results, discuss some relevant observations, and present the conclusions of our study.

II. MODEL AND METHODS

A. Model Hamiltonian

Consider the general form of the Hamiltonian in the vicinity of a Weyl point, along with a possible tilt in the dispersion, given by

$$H_0(k) = w_z k_z + v_x k_x \sigma_x + v_y k_y \sigma_y + v_z k_z \sigma_z, \tag{1}$$

where $\sigma_{x,y,z}$ are the Pauli matrices. The corresponding eigenvalues are

$$E_\pm(k) = w_z k_z \pm \sqrt{v_x^2 k_x^2 + v_y^2 k_y^2 + v_z^2 k_z^2}.$$

The first term is a linear tilting term, which is crucial for the emergence of type-II Weyl fermions. Once $|w_z| > |v_z|$, the Weyl cone is overtilted and the Fermi surface changes from a point to an electron and a hole pocket, touching each other at the type-II Weyl node. Throughout our analysis, we consider $v_x = v_y = v_z = 1$ and tune the tilt parameter w_z, to explore different regimes. When $|w_z| < |v_z| = 1$, we have a conventional type-I Weyl semimetal, while $|w_z| > 1$ corresponds to the overtilted type-II regime. In principle, one could also have a nonlinear dispersion in one or more directions in Eq. (1) above, and include a quadratic tilt term (referred to as a type-III WSM [76]). This model has its own peculiar properties and will be studied in a future work.

For the purpose of our analysis, we study models defined on the cubic lattice. Using Eq. (1) above, we consider the following noninteracting lattice model for a Weyl semimetal with a linear dispersion:

$$H_0 = \sum_k c_k^\dagger (w_z \sin k_z + v_z \sigma_z \sin k_z + v_x \sigma_x \sin k_x + v_y \sigma_y \sin k_y) c_k, \quad (2)$$

where the lattice spacing has been set to unity and the fermion operators are spin doublets, i.e., $c_k \equiv (c_{k\uparrow}, c_{k\downarrow})$. The Weyl nodes for the above model occur at the points (0,0,0), $(\pi, 0, 0)$, $(\pi, \pi, 0)$, and (π, π, π), and permutations thereof. One of the consequences of the presence of Weyl nodes at these high-symmetry points is the absence of Fermi arcs in the usual orthogonal x, y, or z directions. This may be due to the fact that the projected Weyl points on the surfaces in all of these directions are formed by Weyl points of opposite chiralities (see Fig. 5). However, we do see Fermi arcs in the (110) direction for this model. When $w_z = 0$, the above model preserves particle-hole and time-reversal symmetry, as well as C_4 rotational symmetry about the x, y, and z axes, but breaks inversion symmetry. In the presence of a tilt along the z direction, the model continues to preserve particle-hole symmetry, along with C_4 rotational symmetry with respect to the z axis. It should be noted that in the presence of the tilt w_z, we use the particle-hole symmetry operation $c_{k\sigma} \to U_{\sigma\sigma'} c^\dagger_{k\sigma'}$ with $U = i\sigma_z$, leading to $H_0(k) \to -[U^\dagger H_0(-k) U]^*$, augmented by a reflection $k_x \to -k_x$. A similar transformation is also required for the untilted WSM model.

In the real-space representation, the noninteracting Hamiltonian takes the following form:

$$H_0 = \frac{-i}{2} \sum_{r,\alpha\beta} \left(w_z c^\dagger_{r\alpha} c_{r+\hat{z}\beta} + v_z c^\dagger_{r\alpha} \sigma^z_{\alpha\beta} c_{r+\hat{z}\beta} + v_x c^\dagger_{r\alpha} \sigma^x_{\alpha\beta} c_{r+\hat{x}\beta} + v_y c^\dagger_{r\alpha} \sigma^y_{\alpha\beta} c_{r+\hat{y}\beta} \right) - \mu \sum_{r,\sigma} n_{r,\sigma}. \quad (3)$$

Here, $\hat{x}$, $\hat{y}$, and $\hat{z}$ are the lattice unit vectors along the x, y, and z directions, the operator $c_{r\alpha}$ annihilates a particle with spin α on site r, while σ^μ ($\mu = x, y, z$) denotes the three Pauli matrices corresponding to the spin degree of freedom, and the number density per spin projection of the spin-1/2 electrons is $n_{r,\sigma} = c^\dagger_{r,\sigma} c_{r,\sigma}$. In the following analysis, we investigate the effect of local Hubbard interactions on the model defined above. The resulting Hamiltonian is as follows:

$$H = H_0 + U \sum_r n_{r,\uparrow} n_{r,\downarrow}, \quad (4)$$

where H_0 is defined in Eq. (3) above. U is the Hubbard interaction parameter, which is taken to be positive or repulsive. For the purpose of our analysis, the chemical potential is fixed at $\mu = U/2$ throughout, which corresponds to half filling.

As mentioned earlier, we examine the possibility of spin density wave (SDW) orders as prototypical many-body instabilities of the WSM model at half filling with repulsive interactions [77]. A general SDW operator with wave vector Q is defined as follows:

$$\Psi_{\mathrm{SDW}} = \lambda \sum_r A_r \cos[Qr + \phi], \quad (5)$$

where $A_r = S^z_r, S^x_r$, and λ is a variational parameter. In the following analysis, we probe the presence of SDW orders with wave vectors $Q = (\pi, 0, 0)$, $(0, 0, \pi)$, $(\pi, \pi, 0)$, and (π, π, π), and observe stable solutions for different values of Q in the strongly interacting regime, depending on the chosen parameters.

B. Methods: CDMFT and VCA

Here, we provide a brief overview of the quantum cluster methods used in our analysis. For a more detailed discussion of the principles and the mathematical background of these methods, please see Ref. [74].

Cluster dynamical mean-field theory (CDMFT) is an extension of the dynamical mean-field theory (DMFT) method where, instead of a single-site impurity, we consider a cluster of sites with open boundary conditions, taking into account short-range spatial correlations exactly. In this approach, a set of uncorrelated, additional "bath" orbitals hybridized with the cluster are used to account for the effect of the cluster's environment. Thus, the infinite lattice is tiled into small clusters and each of these is coupled to a bath of uncorrelated, auxiliary orbitals. These bath orbitals have their own energy levels $E_{i\sigma}$, which may be spin dependent and are hybridized with the cluster sites r with amplitudes $\Theta_{ir\sigma}$. The bath parameters ($E_{i\sigma}$, $\Theta_{ir\sigma}$) are determined by a self-consistency condition (see Ref. [74] for details).

In our analysis, we use a 12-site (4×8) cluster-bath system, a part of which is illustrated in Fig. 2. An effective model is solved on the cluster, and the self-energy associated with that cluster is then applied to the whole lattice. The lattice Green's function is computed from the cluster's self-energy $\Sigma(\omega)$ as

$$G^{-1}(\tilde{k}, \omega) = G_0^{-1}(\tilde{k}, \omega) - \Sigma(\omega),$$

where $\tilde{k}$ denotes a reduced wave vector (defined in the Brillouin zone of the superlattice) and G_0 is the noninteracting Green's function. Once a solution is found for a given set of model parameters, the above Green's function G can be used to obtain the average values of one-body operators defined on the lattice. An exact-diagonalization solver is used (at zero temperature) and the computational size of the problem is determined by the total number of cluster and bath orbitals. For the type-I WSM model with $|w_z| < 1$, we consider a

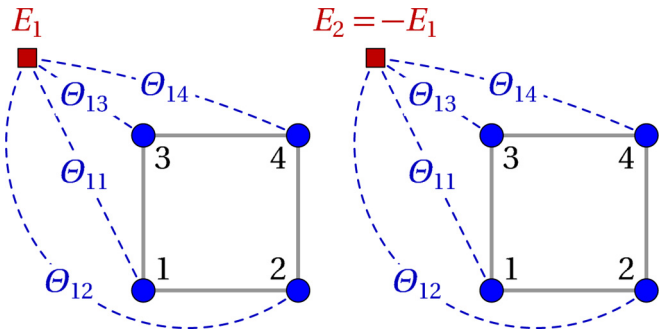

FIG. 2. A part of the 12-site (4 × 8) cluster-bath system used in our CDMFT computations, with 4 cluster sites and 8 bath sites in total, depicting one of the bath sites. For model parameters in the type-I regime, with $|w_z| < 1$, we use a particle-hole symmetric ansatz for the bath parameters, and each cluster site is hybridized with every bath site in the system. This situation is pictorially depicted here. The bath energies are denoted by E_i ($i = 1$–8), and these are hybridized with the cluster sites with hopping amplitudes Θ_{ir} ($i = 1$–8, $r = 1$–4). We consider $E_2 = -E_1$ in this case, as shown above.

particle-hole symmetric ansatz for the bath parameters, and every cluster site is hybridized with every bath site in the system by a hopping parameter. On the other hand, for the type-II WSM model with $|w_z| > 1$, each cluster site is only hybridized with the two bath sites that are adjacent to it, for simplicity. We do not assume other symmetries of the model, such as the C_4 rotational symmetry, during our analysis.

The variational cluster approximation (VCA) method involves solving a model exactly on a small cluster of lattice sites, after inserting fields that represent the effect of the cluster's environment. The essence of this method lies in Potthoff's self-energy functional approach (SFA) [78], involving a functional $\Omega[\Sigma]$ of the self-energy Σ, which is parametrized by the one-body terms collectively labeled by h. The original Hamiltonian H, defined on the infinite lattice, is considered along with a reference Hamiltonian H', which is often a restriction of H to the cluster. In order to probe different broken symmetries, a finite number of Weiss fields may be added to the latter. Any one-body term can be added to H' since the basic requirement is that H' and H must share the same interaction term. The electron self-energy $\Sigma(\omega)$ associated with H' is then used as a variational self-energy to construct the Potthoff self-energy functional (see Ref. [74] for a detailed mathematical explanation of the VCA approach),

$$\Omega[\Sigma(h)] = \Omega'[\Sigma(h)] + \mathrm{Tr}\ln\left\{-\left[G_0^{-1} - \Sigma(h)\right]^{-1}\right\} - \mathrm{Tr}\ln[-G'(h)], \tag{6}$$

where G' is the physical Green's function of the cluster, G_0 is the noninteracting Green's function of the original lattice model, and h jointly denotes the coefficients of the adjustable one-body terms added to H' which act as variational parameters. The symbol Tr stands for a sum over all degrees of freedom and frequencies. Ω' refers to the ground-state energy of the cluster which, along with the associated Green's function G', is computed via the exact-diagonalization method (at zero temperature) in our case. The stationary point of the functional gives the best possible self-energy $\Sigma(\omega)$. This is combined with G_0 to form an approximate Green's function G for the original Hamiltonian H, from which any one-body term, such as the order parameters associated with various SDW orders, can be computed. We define our reference Hamiltonian on an eight-site cubic cluster.

III. RESULTS AND DISCUSSION

In this section, we discuss the behavior of different physical quantities associated with the WSM model defined in Eq. (2), as a function of the interaction strength U, obtained from our analysis. Using CDMFT, we examine the double occupancy $d = \langle n_\uparrow n_\downarrow \rangle$, the relevant SDW order parameters, the spectral function, and the Berry curvature associated with the Weyl nodes, for both the type-I and type-II WSM models. In the VCA approach, we first obtain the behavior of the Potthoff functional Ω as a function of the relevant Weiss fields, corresponding to different types of order. The stationary point of the functional is then used to approximately evaluate the Green's function for the lattice model and calculate different physical properties as a function of the interaction amplitude. We also compare the critical interaction strength for different values of the tilt parameter w_z. Finally, we obtain the interaction-induced phase diagram of the system, as a function of w_z.

A. CDMFT: Numerical results

1. Type I

Here, we discuss our CDMFT results for a type-I Weyl semimetal model, with $v_x = v_y = v_z = 1$ and $w_z = 0$. These results remain qualitatively unchanged for all $|w_z| < |v_z|$.

(a) Double occupancy and order parameter. For the above values of the band structure parameters, our CDMFT solutions indicate that the Weyl semimetal undergoes a continuous transition to the spin density wave (SDW) ordered state $M_z^{(0,0,\pi)} \propto \sum_r S_r^z \cos[Qr + \phi]$ with ordering wave vector $Q = (0, 0, \pi)$ and the magnetization pointing in the z direction, at a critical interaction amplitude $U = U_c \approx 3$. We find clear signatures of a phase transition in the double occupancy, as well as the magnitude of the SDW order parameter $|\langle M_z^{(0,0,\pi)} \rangle|$ calculated as a function of U (see Fig. 3). However, there is an apparent discrepancy between the behavior of these quantities for increasing and decreasing values of U. In the former case, we observe a jump in the double occupancy as well as the order parameter $|\langle M_z^{(0,0,\pi)} \rangle|$, for $U \approx 5 > U_c$. This is evident from Fig. 3(a). However, as we decrease the magnitude of U, no such jump is observed and the transition appears to be continuous. Therefore, an apparent hysteresis behavior is observed in the transition region of $U_{c1} < U < U_{c2}$, where $U_{c1} \approx 3$ and $U_{c2} \approx 5$, which also shows up in the double occupancy. The reason for observing a finite jump in the order parameter is unclear, but it could potentially be due to a false minimum generated in the self-consistency procedure employed in CDMFT, which depends on the direction of the change in U. In the next section, we find that our VCA results clearly point towards a second-order phase transition in this system.

(b) Spectral function. We also calculate the spectral function $A(\omega, k_x, k_y, k_z) = -\frac{1}{\pi}\mathrm{Im}G(\omega, k_x, k_y, k_z)$ for the WSM

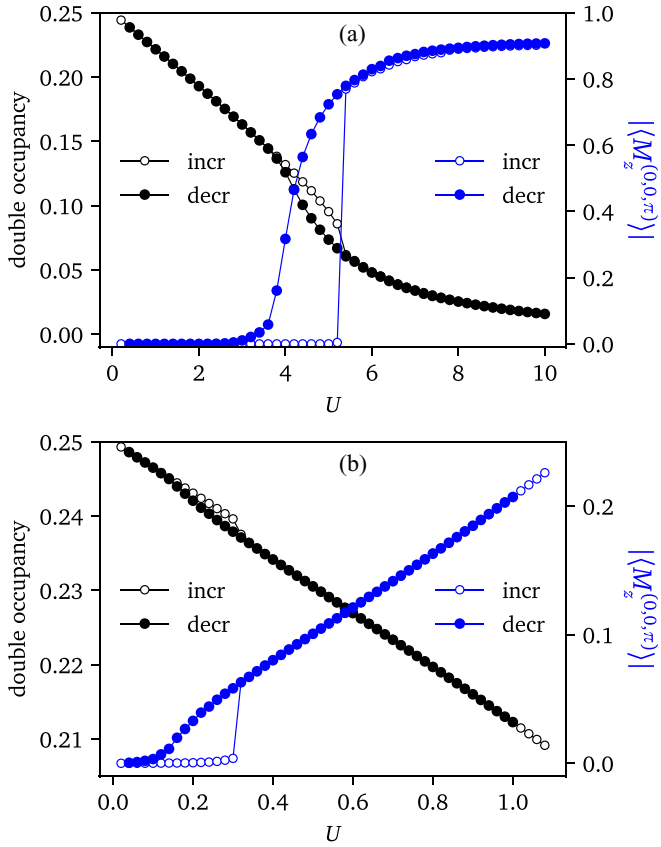

FIG. 3. Evolution of the double occupancy and the spin density wave (SDW) order parameter $\langle M_z^{(0,0,\pi)}\rangle$ with an ordering wave vector $Q = (0, 0, \pi)$, as a function of the interaction parameter U for two sets of model parameters: (a) $v_x = v_y = v_z = 1$, $w_z = 0$ (type I) and (b) $v_x = v_y = v_z = 1$, $w_z = 1.5$ (type II). For the untilted dispersion, this is equivalent to the order $M_x^{(\pi,0,0)}$, with $Q = (\pi, 0, 0)$. In both of the cases, we observe a continuous transition to an SDW ordered state for a critical value of the interaction strength, U_c. For $w_z = 0$, we find $U_c \approx 3$, whereas for $w_z = 1.5 > v_z$, the system reacts much more strongly to the presence of interactions, with $U_c \sim 0.1$. This is expected due to the appearance of a finite Fermi surface for an overtilted dispersion. As explained in the text, we find a jump in the order parameter $\langle M_z^{(0,0,\pi)}\rangle$ as a function of increasing U in our CDMFT calculations for a value of $U > U_c$, which leads to an apparent hysteresis behavior. However, as we decrease U, the system seems to undergo a continuous transition at $U = U_c$.

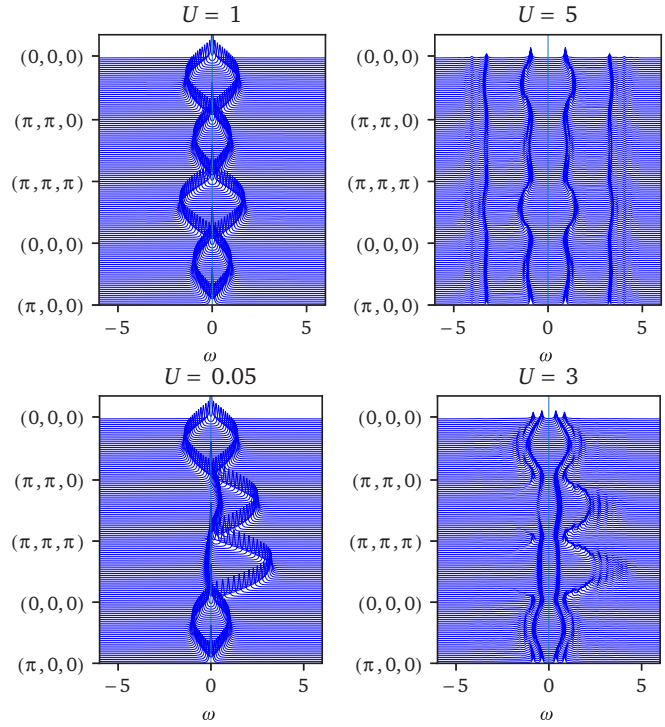

FIG. 4. The spectral function, obtained from our CDMFT calculations, for the gapless Weyl semimetal phase as well as the magnetically ordered phase. The top and bottom panels correspond to the type-I and type-II regime of the parameters, respectively. In the top panels, we present the spectral functions for the band structure parameters $v_x = v_y = v_z = 1$ and $w_z = 0$, considering $U = 1 < U_c$, where the system is still gapless, and $U = 5 > U_c$, where a finite gap has appeared in the spectrum. The bottom panels show the corresponding results for $w_z = 1.5$, with the interaction amplitudes $U = 0.05 < U_c$ and $U = 3 > U_c$. From Fig. 3(b), we observe that the order parameter $\langle M_z^{(0,0,\pi)}\rangle$ varies very slowly as a function of U in the overtilted regime, which may lead to a more gradual appearance of the spectral gap.

model, and illustrate our results for two different values of the interaction parameter U, representative of the semimetallic and $M_z^{(0,0,\pi)}$ phases, respectively (see the top panels in Fig. 4). At $U = 1 < U_c$, the spectrum is found to be gapless, as expected, and the dispersion resembles that of a noninteracting type-I WSM. At $U = 5 > U_c$, a large spectral gap is observed, along with a nontrivial value for the SDW order parameter $\langle M_z^{(0,0,\pi)}\rangle$. This is consistent with the expectation of a phase transition at $U = U_c \approx 3$.

(c) Topological properties. In order to verify the topological properties of the WSM model in the presence of interactions, we calculate the Berry phases associated with the Weyl nodes using an approach introduced in Ref. [46], which we briefly describe below.

In a noninteracting WSM, the Weyl points can be identified as hedgehog singularities of the Berry curvature, $\nabla \times a(k)$, where a is the Berry connection defined in terms of the occupied Bloch states. In the presence of interactions, a many-body Berry connection $A(k)$ and associated Berry curvature $\nabla \times A$ are analogously defined in Ref. [46], using the zero-frequency Green's function. A topological Hamiltonian is defined as

$$H_t(k) = -G(0, k)^{-1} = H(k) + \Sigma(0, k),$$

where H is the Bloch Hamiltonian for the noninteracting case, while $\Sigma(i\omega, k)$ is the self-energy matrix. H_t plays the role of an effective Bloch Hamiltonian for the interacting system and its eigenstates are used to define the many-body Berry connection, as $A(k) = -i\sum\langle nk|\nabla|nk\rangle$, where $H_t(k)|nk\rangle = \widetilde{\epsilon}_n(k)|nk\rangle$, with $\{\widetilde{\epsilon}_n(k)\}$ being the band structure of H_t. Here the sum is restricted to eigenstates with $\widetilde{\epsilon}_n(k) \leqslant 0$. It has been argued that the monopoles of $\nabla \times A$ correspond to the Weyl points of the interacting system.

Using the above approach, we have calculated the Berry curvature for different band structure parameters and a range of values of U. Figure 5 shows the field lines of $\nabla \times A$

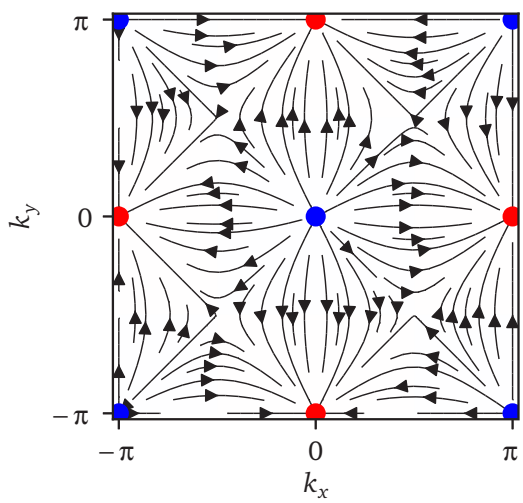

FIG. 5. The field lines of the Berry curvature $\nabla \times A$ in the $k_z = 0$ plane, for the type-I WSM model with parameters $v_x = v_y = v_z = 1$ and $w_z = 0$, considering $U = 2 < U_c$, where the system is still in the semimetallic state. As expected, we obtain the same result in the presence of a finite w_z. In this plane, the Weyl nodes are present at the points (0,0,0), $(\pm\pi, 0, 0)$, $(0, \pm\pi, 0)$, and $(\pm\pi, \pm\pi, 0)$. The directions of the arrows and the colors (red or blue) indicate the chiralities associated with the different nodes. At a critical interaction strength U_c, we observe a transition to an SDW order $M_z^{(0,0,\pi)}$, with an ordering wave vector $Q = (0, 0, \pi)$ [or, equivalently, $M_x^{(\pi,0,0)}$ with $Q = (\pi, 0, 0)$ for $w_z = 0$] which connects Weyl nodes of opposite chiralities. In the ordered state, backfolding due to the ordering wave vector Q maps these Weyl nodes to one another, leading to a gapped spectrum, and the Berry curvature vanishes.

in the $k_z = 0$ plane, for $U = 2 < U_c$, which illustrates the topological properties of the WSM model in the presence of interactions. In the ordered state, we consider a folded Brillouin zone for calculating the Berry curvature, which is found to vanish. Backfolding due to an ordering vector Q maps Weyl nodes to regions of the Brillouin zone with nodes of opposite chirality, where they meet and gap out. We have also verified that the Fermi arcs in this system vanish in the gapped state.

2. Type II (overtilted)

Next, we consider the WSM model in the overtilted type-II regime, i.e., when the tilt parameter $|w_z| > |v_z|$. As an illustrative example, we discuss our results for the band structure parameters $v_x = v_y = v_z = 1$ and $w_z = 1.5$.

(a) Double occupancy and order parameter. When the tilt w_z exceeds a critical value, the Fermi points are replaced by electron and hole pockets touching each other at the type-II Weyl node, the outlines of which can be seen on the $k_x = 0$ plane, along the k_z direction, in Fig. 1(b). Due to the presence of a finite density of states at the Fermi level in this case, the WSM phase is expected to be more susceptible to interaction effects, which is confirmed in our analysis. Here, the system again undergoes a second-order transition to the SDW ordered state $M_z^{(0,0,\pi)}$ (which is no longer equivalent to $M_x^{(\pi,0,0)}$ for $w_z \neq 0$) at a critical value of the interaction $U = U_c$, where $U_c \sim 0.1$. Note that this is significantly diminished in comparison to the previous case, where $U_c \approx 3$. We find that for increasing U, the double occupancy as well as the order parameter $\langle M_z^{(0,0,\pi)} \rangle$ show a small jump at around $U \sim 0.3$, and an apparent hysteresis behavior is again observed in the region $U_{c1} = 0.1 < U < U_{c2} = 0.3$. However, it is found to be less prominent than in the case of a type-I WSM. As we decrease the magnitude of U, no such jump is observed and the transition appears to be continuous [see Fig. 3(b)].

(b) Spectral function. We also show the spectral function obtained in this case for two representative values of U, i.e., $U = 0.05 < U_c$ and $U = 3 > U_c$, in the bottom panels in Fig. 4. In this case, we find a relatively gradual opening of the spectral gap, as compared to the top panels with $w_z = 0$, which may be due to a much slower variation in the magnitude of the order parameter $\langle M_z^{(0,0,\pi)} \rangle$ in this case.

To conclude this part of our analysis, our CDMFT solutions for the WSM model in Eq. (2), with interactions, indicate a second-order phase transition to a spin density wave ordered state at a critical interaction strength $U = U_c$. This is accompanied by the appearance of a gap in the spectral function and the vanishing of the Berry curvature associated with the Weyl nodes. For both the type-I and type-II WSM models considered above, we observe an apparent jump in the magnitude of the order parameter for increasing values of U, which is absent for decreasing U. This could be due to a false minimum in the CDMFT procedure, which is prone to first-order transitions. The SDW order is found to become more robust for larger values of U, as indicated by a slow increase in the magnitude of the order parameter for $U > U_c$. In the next section, we confirm the order of the transition using the VCA approach.

B. VCA: Numerical results

We have also used the variational cluster approximation (VCA) method to investigate the effect of local repulsive interactions on the WSM model. As stated earlier, we limit our considerations to spin density wave instabilities, and probe the relevant SDW orders by solving the following Hamiltonian on an eight-site cubic cluster:

$$H' = H_0' + hM_z^{(0,0,\pi)\prime},$$

where H_0' and $M_z^{(0,0,\pi)\prime}$ are the restriction to the cluster of the kinetic-energy operator, and the SDW operator $M_z^{(0,0,\pi)}$ defined in Eq. (5), respectively. The coefficient h is the corresponding Weiss field, which is the variational parameter used in optimizing the Potthoff functional Ω. We study the evolution of the Potthoff functional Ω, as a function of h, for different values of U. Initially, for a weakly interacting system, Ω has a single minimum at $h = 0$, indicating the absence of the corresponding SDW order. At a critical value $U = U_c$, it develops a new minimum at a finite value of the Weiss field h, along with a maximum at $h = 0$, and this behavior of Ω confirms the continuous nature of the WSM-SDW transition. The approximate Green's function for the lattice model, determined by the stationary point of Ω, is then used to evaluate the order parameter $\langle M_z^{(0,0,\pi)} \rangle$ as a function of U.

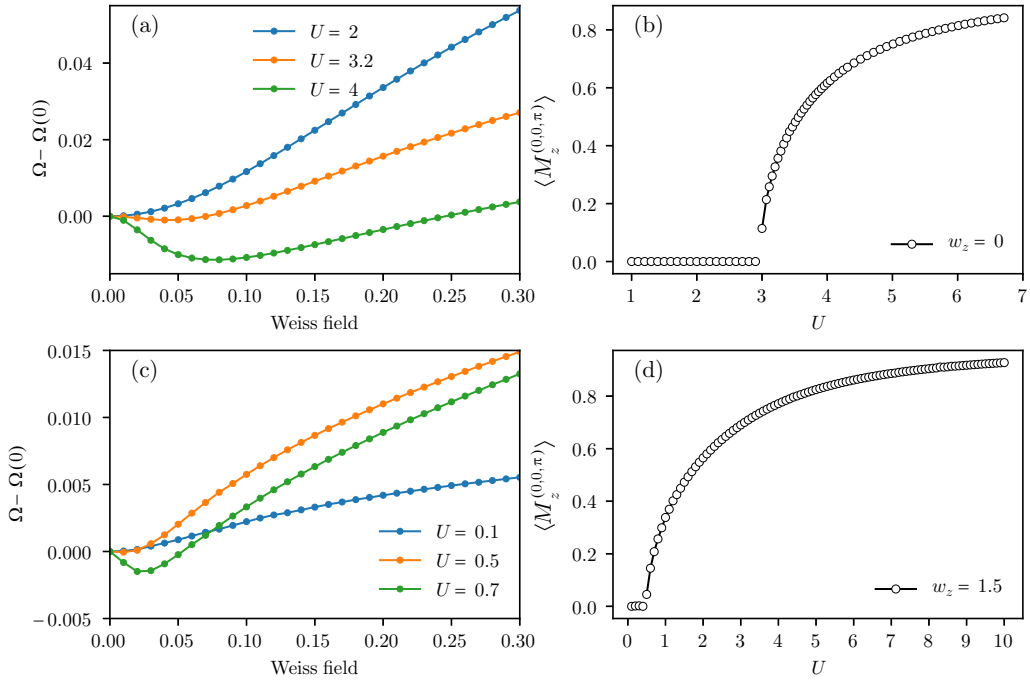

FIG. 6. (a) Behavior of the Potthoff functional Ω as a function of the Weiss field h for different values of U (in the vicinity of the critical interaction U_c) for the type-I WSM with model parameters $v_x = v_y = v_z = 1$ and $w_z = 0$. (b) Evolution of the SDW order parameter $\langle M_z^{(0,0,\pi)} \rangle$ as a function of U, obtained from our VCA calculations. (c),(d) Corresponding results for the type-II WSM model, with $v_x = v_y = v_z = 1$ and $w_z = 1.5$. We find that for both these models, the Potthoff functional Ω develops a minimum at a nonzero value of the Weiss field h, at a critical value of the interaction strength, $U = U_c$. This is an indication of a continuous transition to the corresponding ordered state. The behavior of the order parameter $\langle M_z^{(0,0,\pi)} \rangle$ as a function of U, obtained from the VCA approach, also indicates a second-order transition at $U = U_c$. Note that the value of U_c depends sensitively on the tilt parameter w_z and is significantly diminished in the parameter regime where $|w_z| > 1$.

Finally, we present the interaction-induced phase diagram of the WSM model, as a function of the tilt w_z.

1. Type I

Here, we describe the VCA results for a type-I WSM model with parameters $v_x = v_y = v_z = 1$ and $w_z = 0$. Figure 6(a) shows the behavior of the Potthoff functional Ω as a function of the Weiss field h for different values of U. For $U < U_c$, Ω has a single minimum at $h = 0$, corresponding to the gapless semimetallic state. At $U \approx 3 = U_c$, it develops a new minimum at a finite value of h (with a maximum at $h = 0$), indicating a continuous transition to the corresponding magnetically ordered state. We then use the corresponding solution to calculate various physical properties of the model and, in particular, the order parameter $\langle M_z^{(0,0,\pi)} \rangle$ as a function of U, which becomes nonzero at the critical value $U = U_c$, as illustrated in Fig. 6(b). The magnitude of $\langle M_z^{(0,0,\pi)} \rangle$ increases slowly as a function of U and is found to be sensitive to the band structure parameters.

2. Type II (overtilted)

Here, we discuss our VCA results for the WSM model parameters $v_x = v_y = v_z = 1$ and $w_z = 1.5$. We find that the Potthoff functional Ω once again develops a minimum at a nonzero value of the Weiss field h, with a maximum at $h = 0$, for a critical interaction strength $U_c \sim 0.7$ [see Fig. 6(c)], which is significantly lower than the one obtained for the type-I regime. The solution corresponding to the stationary point of Ω is used to calculate the order parameter $\langle M_z^{(0,0,\pi)} \rangle$ as a function of U [see Fig. 6(d)] . Overall, the behavior of the system in this regime is found to be qualitatively similar to that of the type-I WSM model, though evidently more sensitive to interaction effects. This is qualitatively consistent with the CDMFT results obtained for this model.

In Fig. 7, we use our VCA results for different sets of band structure parameters to plot the magnitude of the order parameter $\langle M_z^{(0,0,\pi)} \rangle$ as a function of U, for different values of w_z. As the tilt w_z is increased, the critical interaction strength U_c decreases. In particular, we find a significant change in the value of U_c when $|w_z| > 1 = |v_z|$. Figure 8 shows the interaction-induced phase diagram for the WSM model defined in Eq. (2), as a function of the parameter w_z, for $v_x = v_y = v_z = 1$. The value of the tilt parameter w_z, at which the system undergoes a transition from the type-I to the type-II regime (dictated by a singularity in derivative of the critical interaction U_c), is also found to be slightly renormalized in the presence of interactions, as indicated by the dashed red line in Fig. 8. In general, for a nontrivial tilt term, the position in the phase diagram where the order appears is highly sensitive to the magnitude of the tilt, and the nature of the SDW order may depend on its direction.

To conclude this part, we find from our VCA analysis that the WSM model defined by us in Sec. II shows a continuous transition to an SDW ordered state at a critical value of the interaction strength U_c, which is particularly sensitive to the

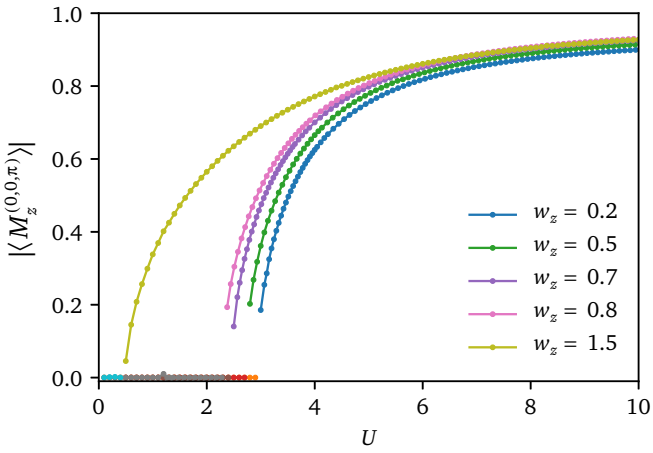

FIG. 7. Evolution of the SDW order parameter $\langle M_z^{(0,0,\pi)}\rangle$ as a function of the interaction strength U, obtained from our VCA calculations, for different values of the tilt parameter w_z, with $v_x = v_y = v_z = 1$. Note that as the magnitude of w_z increases, the magnetic transition is found to occur at smaller values of $U = U_c$, which implies that the semimetallic phase is now more susceptible to interactions. In particular, once in the overtilted type-II regime, i.e., $|w_z| > |v_z|$, we find a sharp decrease in the critical value of the interaction U_c due to the appearance of a finite Fermi surface with neighboring electron and hole pockets. This change is also evident from the behavior of the critical interaction U_c as a function of w_z, plotted in Fig. 8.

magnitude of the tilt parameter, and this order becomes more robust for increasing values of U.

IV. CONCLUSIONS

In summary, we have studied the effect of a local repulsive interaction U on an inversion-symmetry breaking Weyl semimetal (WSM) model using the cluster dynamical mean-

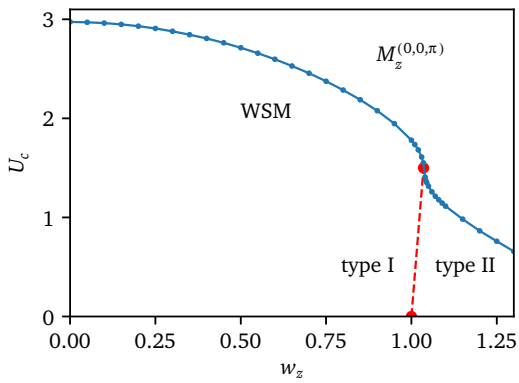

FIG. 8. The interaction-induced phase diagram for the Weyl semimetal model defined in Eq. (2), as a function of the tilt parameter w_z and the corresponding critical interaction U_c. The latter determines the phase boundary between the WSM and $M_z^{(0,0,\pi)}$ (SDW) phases for increasing values of $|w_z|$. For increasing values of w_z, the critical interaction strength for the transition is found to decrease. We find a singularity in the derivative of U_c, which indicates the appearance of a finite Fermi surface in the overtilted type-II regime. The dashed red line demarcates the transition between the type-I and type-II regimes.

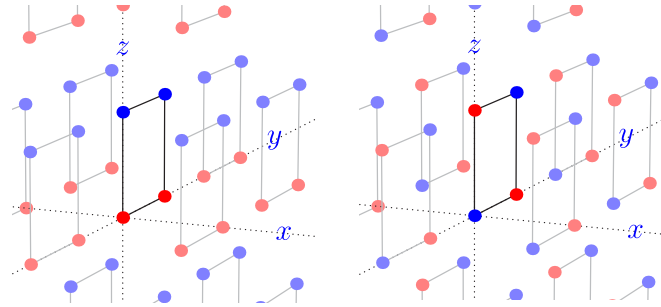

FIG. 9. The arrangement of the four-site clusters employed for our CDMFT calculations, with superlattice vectors that can accommodate the SDW orders considered by us, i.e., (a) $M_z^{(0,0,\pi)}$ with wave vector $Q = (0, 0, \pi)$ and (b) $M_z^{(\pi,\pi,\pi)}$ with wave vector $Q = (\pi, \pi, \pi)$. Here, we consider a cluster of side α, where α is the lattice constant and the superlattice vectors are (1,1,0), (0,2,0), and (0,0,2), with distances measured in units of α.

field theory (CDMFT) and variational cluster approximation (VCA) methods. We examine the evolution of the system as a function of the interaction strength U, taking into account the effect of a nonzero tilt parameter w_z. We find that the system undergoes a second-order transition at a critical value of the interaction $U = U_c$, to a spin density wave (SDW) ordered state, with an ordering wave vector $Q = (0, 0, \pi)$ and magnetization in the z direction (see Figs. 9 and 10). For the untilted dispersion, this is equivalent to the corresponding state with a wave vector $Q = (\pi, 0, 0)$ and magnetization in the x direction. These wave vectors connect Weyl nodes of opposite chiralities, and such instabilities are favored by the nesting between these points in the band structure. This result makes sense from a physical point of view since the Weyl nodes are pinned to high-symmetry points in our model, preventing the movement of nodes of opposite chiralities towards each other. The phase transition is accompanied by the gradual appearance of a gap in the spectrum. The Berry flux associated with the Weyl nodes is also found to disappear in the ordered state due to the backfolding of the Weyl nodes with opposite chiralities onto each other.

In the type-II or overtilted regime, the corresponding phase transition occurs at a significantly lower value of U_c, indicating that the WSM phase is more susceptible to interactions in this case. The nature of the transition as well as the magnetic order is confirmed by the results of our VCA calculations. We then obtain the ground-state phase diagram for the WSM model, as a function of the tilt parameter w_z, and find that the critical value of the tilt at which the system undergoes a transition from the type-I to the type-II WSM phase is renormalized in the presence of interactions. Spin density wave instabilities have also appeared in previous studies on type-I and type-II Weyl semimetal models, as well as Dirac semimetal models, using different methods [42,43,49,50,53,79–81], primarily analytical.

There has been a handful of studies in the literature on the interaction effects in Weyl semimetals, which have employed quantum cluster methods [43,46,82]; a prominent example, similar in spirit to our work, is Ref. [43], where the VCA

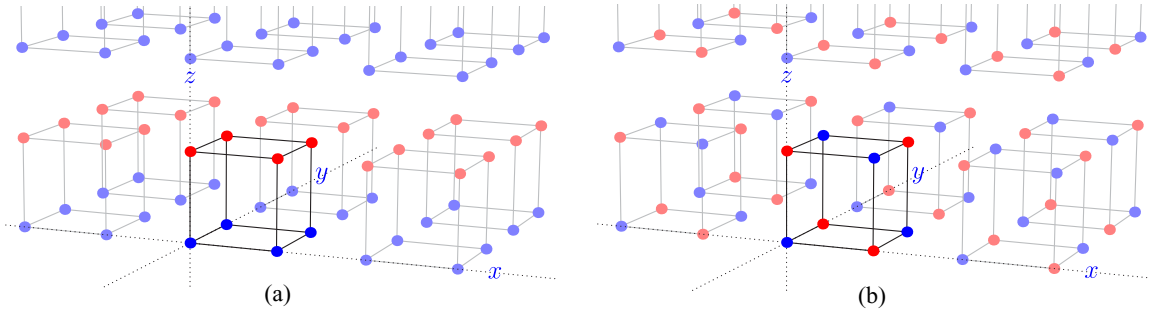

FIG. 10. The eight-site cubic cluster employed by us for our VCA computations with an illustration of the competing solutions for SDW orders, i.e., (a) $M_z^{(0,0,\pi)}$ with wave vector $Q = (0, 0, \pi)$ and (b) $M_z^{(\pi,\pi,\pi)}$ with wave vector $Q = (\pi, \pi, \pi)$. Here, we consider a cluster of side α, where α is the lattice constant, and the superlattice vectors are (2,0,0), (0,2,0), and (0,0,2), with distances measured in units of α.

approach is used to investigate the effect of both repulsive and attractive interactions on a time-reversal symmetry breaking type-I WSM model with tetragonal symmetry, using a slab geometry. Unlike in the model used by us, the specific symmetries and structure of this model allow the positions of the Weyl nodes to be unrestricted along one of the directions in momentum space. Unlike Ref. [43], we also employ the CDMFT approach for our analysis, which is useful for studying a possible Mott insulating phase. As mentioned earlier, we restrict ourselves to the consideration of repulsive interactions at half filling and, more generally, for longer-range or attractive interactions, one should take into account competing instabilities, such as charge density wave and superconducting states. While the quantum cluster methods used in this analysis have the advantage of being nonperturbative and are especially useful in the strongly interacting limit, they only take into account short-range correlations and may therefore overemphasize the order.

Our treatment may easily be generalized to more complicated Weyl semimetal models, such as for multi-Weyl systems with quadratic tilt terms, and such problems will be addressed in future studies.

ACKNOWLEDGMENTS

Computing resources were provided by Compute Canada and Calcul Québec.

APPENDIX: EFFECTIVE HAMILTONIAN AT LARGE U

We use the strong-coupling expansion method to obtain the effective spin Hamiltonian for our model in the large-U limit. For $w_z = 0$, the effective Hamiltonian is given by

$$\begin{aligned} H_{\text{eff}} = & J_z \sum_{\langle ij\rangle_z} \left(S_i^z S_j^z - S_i^x S_j^x - S_i^y S_j^y\right) \\ & + J_x \sum_{\langle ij\rangle_x} \left(-S_i^z S_j^z + S_i^x S_j^x - S_i^y S_j^y\right) \\ & + J_y \sum_{\langle ij\rangle_y} \left(-S_i^z S_j^z - S_i^x S_j^x + S_i^y S_j^y\right), \end{aligned}$$

where $J_x = J_y = \frac{4v_x^2}{U}$, $J_y = \frac{4v_y^2}{U}$, and $J_z = \frac{4v_z^2}{U}$ in terms of our WSM model parameters. For $J_z \gg J_x$, a ferromagnetic order along z is favored with spins in the xy plane, with an antiferromagnetic order along $(\pi, 0, 0)$, as a correction, if $\mathbf{S}$ is along x. The same behavior would be observed in the other two directions if we have $J_x \gg J_z$, for instance, so the ratios $\frac{J_z}{J_x}$ or $\frac{J_z}{J_y}$ do not have a qualitative effect on the behavior of the above Hamiltonian. This is consistent with the equivalence that we observe, for $w_z = 0$, between the SDW order $M_z^{(0,0,\pi)}$ [with wave vector $(0, 0, \pi)$ and magnetization in the z direction] and $M_x^{(\pi,0,0)}$ [with wave vector $(\pi, 0, 0)$ and magnetization in the x direction]. However, we find no such equivalence to be present in either the noninteracting or the large-U limit, when $w_z \neq 0$.

[1] W. Witczak-Krempa, G. Chen, Y. B. Kim, and L. Balents, Annu. Rev. Condens. Matter Phys. **5**, 57 (2014).
[2] J. G. Rau, E. K.-H. Lee, and H.-Y. Kee, Annu. Rev. Condens. Matter Phys. **7**, 195 (2016).
[3] R. Schaffer, E. K.-H. Lee, B.-J. Yang, and Y. B. Kim, Rep. Prog. Phys. **79**, 094504 (2016).
[4] Y. Ando and L. Fu, Annu. Rev. Condens. Matter Phys. **6**, 361 (2015).
[5] M. Z. Hasan and J. E. Moore, Annu. Rev. Condens. Matter Phys. **2**, 55 (2011).
[6] Y. Ando, J. Phys. Soc. Jpn. **82**, 102001 (2013).
[7] M. Z. Hasan, S.-Y. Xu, and G. Bian, Phys. Scr. **T164**, 014001 (2015).
[8] M. Z. Hasan and C. L. Kane, Rev. Mod. Phys. **82**, 3045 (2010).
[9] X.-L. Qi and S.-C. Zhang, Rev. Mod. Phys. **83**, 1057 (2011).
[10] B. Yan and S.-C. Zhang, Rep. Prog. Phys. **75**, 096501 (2012).
[11] B. Yan and C. Felser, Annu. Rev. Condens. Matter Phys. **8**, 337 (2017).
[12] O. Vafek and A. Vishwanath, Annu. Rev. Condens. Matter Phys. **5**, 83 (2014).
[13] S. Jia, S.-Y. Xu, and M. Z. Hasan, Nat. Mater. **15**, 1140 (2016).
[14] N. P. Armitage, E. J. Mele, and A. Vishwanath, Rev. Mod. Phys. **90**, 015001 (2018).
[15] K. Deng, G. Wan, P. Deng, K. Zhang, S. Ding, E. Wang, M. Yan, H. Huang, H. Zhang, Z. Xu, J. Denlinger, A. Fedorov,

H. Yang, W. Duan, H. Yao, Y. Wu, S. Fan, H. Zhang, X. Chen, and S. Zhou, Nat. Phys. **12**, 1105 (2016).
[16] S.-M. Huang, S.-Y. Xu, I. Belopolski, C.-C. Lee, G. Chang, B. Wang, N. Alidoust, G. Bian, M. Neupane, C. Zhang, S. Jia, A. Bansil, H. Lin, and M. Z. Hasan, Nat. Commun. **6**, 7373 (2015).
[17] I. Belopolski, S.-Y. Xu, D. S. Sanchez, G. Chang, C. Guo, M. Neupane, H. Zheng, C.-C. Lee, S.-M. Huang, G. Bian, N. Alidoust, T.-R. Chang, B. K. Wang, X. Zhang, A. Bansil, H.-T. Jeng, H. Lin, S. Jia, and M. Z. Hasan, Phys. Rev. Lett. **116**, 066802 (2016).
[18] A. C. Potter, I. Kimchi, and A. Vishwanath, Nat. Commun. **5**, 5161 (2014).
[19] S.-Y. Xu, I. Belopolski, N. Alidoust, M. Neupane, G. Bian, C. Zhang, R. Sankar, G. Chang, Z. Yuan, C.-C. Lee, S.-M. Huang, H. Zheng, J. Ma, D. S. Sanchez, B. Wang, A. Bansil, F. Chou, P. P. Shibayev, H. Lin, S. Jia, and M. Z. Hasan, Science **349**, 613 (2015).
[20] D.-F. Xu, Y.-P. Du, Z. Wang, Y.-P. Li, X.-H. Niu, Q. Yao, D. Pavel, Z.-A. Xu, X.-G. Wan, and D.-L. Feng, Chin. Phys. Lett. **32**, 107101 (2015).
[21] A. A. Zyuzin and A. A. Burkov, Phys. Rev. B **86**, 115133 (2012).
[22] Z. Wang and S.-C. Zhang, Phys. Rev. B **87**, 161107(R) (2013).
[23] G. Sharma, P. Goswami, and S. Tewari, Phys. Rev. B **96**, 045112 (2017).
[24] S. A. Parameswaran, T. Grover, D. A. Abanin, D. A. Pesin, and A. Vishwanath, Phys. Rev. X **4**, 031035 (2014).
[25] X. Huang, L. Zhao, Y. Long, P. Wang, D. Chen, Z. Yang, H. Liang, M. Xue, H. Weng, Z. Fang, X. Dai, and G. Chen, Phys. Rev. X **5**, 031023 (2015).
[26] C.-L. Zhang, S.-Y. Xu, I. Belopolski, Z. Yuan, Z. Lin, B. Tong, G. Bian, N. Alidoust, C.-C. Lee, S.-M. Huang, T.-R. Chang, G. Chang, C.-H. Hsu, H.-T. Jeng, M. Neupane, D. S. Sanchez, H. Zheng, J. Wang, H. Lin, C. Zhang, H.-Z. Lu, S.-Q. Shen, T. Neupert, M. Zahid Hasan, and S. Jia, Nat. Commun. **7**, 10735 (2016).
[27] A. A. Soluyanov, D. Gresch, Z. Wang, Q. Wu, M. Troyer, X. Dai, and B. A. Bernevig, Nature (London) **527**, 495 (2015).
[28] J. Jiang, Z. Liu, Y. Sun, H. Yang, C. Rajamathi, Y. Qi, L. Yang, C. Chen, H. Peng, C.-C. Hwang, S. Sun, S.-K. Mo, I. Vobornik, J. Fujii, S. Parkin, C. Felser, B. Yan, and Y. Chen, Nat. Commun. **8**, 13973 (2017).
[29] M. Alidoust, K. Halterman, and A. A. Zyuzin, Phys. Rev. B **95**, 155124 (2017).
[30] M. Udagawa and E. J. Bergholtz, Phys. Rev. Lett. **117**, 086401 (2016).
[31] A. A. Zyuzin and R. Tiwari, JETP Lett. **103**, 717 (2016).
[32] Y. Wu, D. Mou, N. H. Jo, K. Sun, L. Huang, S. L. Bud'ko, P. C. Canfield, and A. Kaminski, Phys. Rev. B **94**, 121113(R) (2016).
[33] Y. Qi, P. G. Naumov, M. N. Ali, C. R. Rajamathi, W. Schnelle, O. Barkalov, M. Hanfland, S.-C. Wu, C. Shekhar, Y. Sun, V. Süß, M. Schmidt, U. Schwarz, E. Pippel, P. Werner, R. Hillebrand, T. Förster, E. Kampert, S. Parkin, R. J. Cava, C. Felser, B. Yan, and S. A. Medvedev, Nat. Commun. **7**, 11038 (2016).
[34] S.-Y. Xu, N. Alidoust, I. Belopolski, Z. Yuan, G. Bian, T.-R. Chang, H. Zheng, V. N. Strocov, D. S. Sanchez, G. Chang, C. Zhang, D. Mou, Y. Wu, L. Huang, C.-C. Lee, S.-M. Huang, B. Wang, A. Bansil, H.-T. Jeng, T. Neupert, A. Kaminski, H. Lin, S. Jia, and M. Zahid Hasan, Nat. Phys. **11**, 748 (2015).
[35] N. Xu, H. M. Weng, B. Q. Lv, C. E. Matt, J. Park, F. Bisti, V. N. Strocov, D. Gawryluk, E. Pomjakushina, K. Conder, N. C. Plumb, M. Radovic, G. Autès, O. V. Yazyev, Z. Fang, X. Dai, T. Qian, J. Mesot, H. Ding, and M. Shi, Nat. Commun. **7**, 11006 (2016).
[36] S.-Y. Xu, I. Belopolski, D. S. Sanchez, C. Zhang, G. Chang, C. Guo, G. Bian, Z. Yuan, H. Lu, T.-R. Chang, P. P. Shibayev, M. L. Prokopovych, N. Alidoust, H. Zheng, C.-C. Lee, S.-M. Huang, R. Sankar, F. Chou, C.-H. Hsu, H.-T. Jeng, A. Bansil, T. Neupert, V. N. Strocov, H. Lin, S. Jia, and M. Z. Hasan, Sci. Adv. **1**, e1501092 (2015).
[37] L. X. Yang, Z. K. Liu, Y. Sun, H. Peng, H. F. Yang, T. Zhang, B. Zhou, Y. Zhang, Y. F. Guo, M. Rahn, D. Prabhakaran, Z. Hussain, S.-K. Mo, C. Felser, B. Yan, and Y. L. Chen, Nat. Phys. **11**, 728 (2015).
[38] Y. Li, Y. Zhou, Z. Guo, F. Han, X. Chen, P. Lu, X. Wang, C. An, Y. Zhou, J. Xing, G. Du, X. Zhu, H. Yang, J. Sun, Z. Yang, W. Yang, H.-K. Mao, Y. Zhang, and H.-H. Wen, npj Quantum Mater. **2**, 66 (2017).
[39] Q. Wang, Y. Xu, R. Lou, Z. Liu, M. Li, Y. Huang, D. Shen, H. Weng, S. Wang, and H. Lei, Nat. Commun. **9**, 3681 (2018).
[40] P. Puphal, V. Pomjakushin, N. Kanazawa, V. Ukleev, D. J. Gawryluk, J. Ma, M. Naamneh, N. C. Plumb, L. Keller, R. Cubitt, E. Pomjakushina, and J. S. White, Phys. Rev. Lett. **124**, 017202 (2020).
[41] M.-F. Yang, Phys. Rev. B **100**, 245137 (2019).
[42] L.-J. Zhai, P.-H. Chou, and C.-Y. Mou, Phys. Rev. B **94**, 125135 (2016).
[43] M. Laubach, C. Platt, R. Thomale, T. Neupert, and S. Rachel, Phys. Rev. B **94**, 241102(R) (2016).
[44] F. Xue and X.-X. Zhang, Phys. Rev. B **96**, 195160 (2017).
[45] J. Carlström and E. J. Bergholtz, Phys. Rev. B **98**, 241102(R) (2018).
[46] W. Witczak-Krempa, M. Knap, and D. Abanin, Phys. Rev. Lett. **113**, 136402 (2014).
[47] K. Li, Phys. Rev. B **102**, 165150 (2020).
[48] H. Wei, S.-P. Chao, and V. Aji, Phys. Rev. B **89**, 014506 (2014).
[49] H. Wei, S.-P. Chao, and V. Aji, Phys. Rev. B **89**, 235109 (2014).
[50] J. Maciejko and R. Nandkishore, Phys. Rev. B **90**, 035126 (2014).
[51] B. Roy, P. Goswami, and V. Juričić, Phys. Rev. B **95**, 201102(R) (2017).
[52] Y.-L. Lee and Y.-W. Lee, Phys. Rev. B **96**, 045115 (2017).
[53] Y.-X. Wang, F. Li, and B. Bian, Phys. Rev. B **96**, 165203 (2017).
[54] H. Wei, S.-P. Chao, and V. Aji, Phys. Rev. Lett. **109**, 196403 (2012).
[55] L. Crippa, A. Amaricci, N. Wagner, G. Sangiovanni, J. C. Budich, and M. Capone, Phys. Rev. Res. **2**, 012023(R) (2020).
[56] W. Yi, Q.-S. Wang, R. Wang, and B. Wang, arXiv:1707.09576.
[57] S.-X. Zhang, S.-K. Jian, and H. Yao, arXiv:1809.10686.
[58] A. Sharma, A. Scammell, J. Krieg, and P. Kopietz, Phys. Rev. B **97**, 125113 (2018).
[59] A. Sekine and K. Nomura, J. Phys. Soc. Jpn. **83**, 094710 (2014).
[60] T. Meng and J. C. Budich, Phys. Rev. Lett. **122**, 046402 (2019).
[61] I. Boettcher, Phys. Rev. Lett. **124**, 127602 (2020).
[62] C. Berke, P. Michetti, and C. Timm, New J. Phys. **20**, 043057 (2018).
[63] T. Zhou, Y. Gao, and Z. D. Wang, Phys. Rev. B **93**, 094517 (2016).

[64] G. Bednik, A. A. Zyuzin, and A. A. Burkov, Phys. Rev. B **92**, 035153 (2015).
[65] J. Carlström and E. J. Bergholtz, Phys. Rev. B **97**, 161102(R) (2018).
[66] O. Parcollet, G. Biroli, and G. Kotliar, Phys. Rev. Lett. **92**, 226402 (2004).
[67] H. Park, K. Haule, and G. Kotliar, Phys. Rev. Lett. **101**, 186403 (2008).
[68] Y. Nomura, S. Sakai, and R. Arita, Phys. Rev. B **91**, 235107 (2015).
[69] A. I. Lichtenstein and M. I. Katsnelson, Phys. Rev. B **62**, R9283 (2000).
[70] C. Dahnken, M. Aichhorn, W. Hanke, E. Arrigoni, and M. Potthoff, Phys. Rev. B **70**, 245110 (2004).
[71] A. Payeur and D. Sénéchal, Phys. Rev. B **83**, 033104 (2011).
[72] M. Potthoff, M. Aichhorn, and C. Dahnken, Phys. Rev. Lett. **91**, 206402 (2003).
[73] T. Shirakawa, H. Watanabe, and S. Yunoki, J. Phys.: Conf. Ser. **273**, 012148 (2011).
[74] D. Sénéchal, arXiv:0806:2690.
[75] G. Biroli and G. Kotliar, Phys. Rev. B **65**, 155112 (2002).
[76] X.-P. Li, K. Deng, B. Fu, Y. Li, D. Ma, J. Han, J. Zhou, S. Zhou, and Y. Yao, arXiv:1909.12178.
[77] While superconductivity and charge density wave order are ruled out due to these conditions, we have also examined the possibility of on-site and bond ferromagnetism, which are not found to occur in this model.
[78] *Strongly Correlated Systems*, edited by A. Avella and F. Mancini, Springer Series in Solid-State Sciences Vol. 171 (Springer, Berlin & Heidelberg, 2011).
[79] Y. Wang and P. Ye, Phys. Rev. B **94**, 075115 (2016).
[80] N. S. Srivatsa and R. Ganesh, Phys. Rev. B **98**, 165133 (2018).
[81] G. Bednik, Phys. Rev. B **102**, 125119 (2020).
[82] K. Jing, Z. Jianfei, L. Kai, Y. Shun-Li, and S. Lu-Bing, Sci. Rep. **9**, 2824 (2019).